REPORT DOCUMENTATION PAGE

Form Approved OMB NO. 0704-0188

1. REPORT DATE (DD-MM-YYYY)	2. REPORT TYPE	3. DATES COVERED (From - To)
11-06-2014	Final Report	1-Sep-2013 - 31-May-2014

4. TITLE AND SUBTITLE
Untangling the Reaction Mechanisms Involved in the Explosive Decomposition of Model Compounds of Energetic Materials

5a. CONTRACT NUMBER
W911NF-13-1-0424

5b. GRANT NUMBER

5c. PROGRAM ELEMENT NUMBER
611102

6. AUTHORS
Ralf I. Kaiser

5d. PROJECT NUMBER

5e. TASK NUMBER

5f. WORK UNIT NUMBER

7. PERFORMING ORGANIZATION NAMES AND ADDRESSES
University of Hawaii - Hilo
2530 Dole Street
Sakamaki D-200
Honolulu, HI 96822 -2309

8. PERFORMING ORGANIZATION REPORT NUMBER

9. SPONSORING/MONITORING AGENCY NAME(S) AND ADDRESS (ES)
U.S. Army Research Office
P.O. Box 12211
Research Triangle Park, NC 27709-2211

10. SPONSOR/MONITOR'S ACRONYM(S)
ARO

11. SPONSOR/MONITOR'S REPORT NUMBER(S)
61380-CH-II.1

12. DISTRIBUTION AVAILIBILITY STATEMENT
Approved for Public Release; Distribution Unlimited

13. SUPPLEMENTARY NOTES
The views, opinions and/or findings contained in this report are those of the author(s) and should not contrued as an official Department of the Army position, policy or decision, unless so designated by other documentation.

14. ABSTRACT
We investigated the electron- and photon- (10.5 eV) induced decomposition of nitromethane (CH_3NO_2) in the condensed phase at 5 K. Infrared spectroscopically, we identified four newly formed molecules in irradiated (D3)-nitromethane ice films: CH_3ONO, H_2CO, NO, and HNO. The data analysis suggest first order kinetics of the formation of methyl nitrite (CH_3ONO) via isomerization of nitromethane (CH_3NO_2) (k1). Both the methyl radical and the nitrogen dioxide formed via the carbon-nitrogen bond rupture are trapped within the matrix cage and recombine back to nitromethane (CH_3NO_2) or form methylnitrite (CH_3ONO). The isomerization of D3

15. SUBJECT TERMS
energetic material reaction dynamics decomposition mechsnism

16. SECURITY CLASSIFICATION OF:			17. LIMITATION OF ABSTRACT	15. NUMBER OF PAGES	19a. NAME OF RESPONSIBLE PERSON
a. REPORT	b. ABSTRACT	c. THIS PAGE			Ralf Kaiser
UU	UU	UU	UU		19b. TELEPHONE NUMBER 808-956-5731

Report Title

Untangling the Reaction Mechanisms Involved in the Explosive Decomposition of Model Compounds of Energetic Materials

ABSTRACT

We investigated the electron- and photon- (10.5 eV) induced decomposition of nitromethane (CH3NO2) in the condensed phase at 5 K. Infrared spectroscopically, we identified four newly formed molecules in irradiated (D3)-nitromethane ice films: CH3ONO, H2CO, NO, and HNO. The data analysis suggest first order kinetics of the formation of methyl nitrite (CH3ONO) via isomerization of nitromethane (CH3NO2) (k1). Both the methyl radical and the nitrogen dioxide formed via the carbon-nitrogen bond rupture are trapped within the matrix cage and recombine back to nitromethane (CH3NO2) or form methylnitrite (CH3ONO). The isomerization of D3-nitromethane is faster than of nitromethane with k1(CD3NO2)/k1(CH3NO2) = 2.0 ± 0.8 proposing non-equilibrium reaction dynamics. Methylnitrite (CH3ONO) decomposed via two competing pathways into formaldehyde (H2CO) plus nitrosyl hydride (HNO) and the methoxy radical (CH3O) plus nitrogen monoxide (NO). The dominance of the molecular product channel is quite distinct from the gas phase experiments depicting a prevailing radical channel. Reflectron time-of-flight mass spectroscopy coupled to single photon ionization revealed that the reaction mechanisms in the condensed phase are more complex than in the gas phase. These involve addition of suprathermal hydrogen atoms (leading eventually to H2NOH), radical-radical recombination reactions (CH3NO), and pathways leading to hydroxymethylamine (CH3NHOH).

Enter List of papers submitted or published that acknowledge ARO support from the start of the project to the date of this printing. List the papers, including journal references, in the following categories:

(a) Papers published in peer-reviewed journals (N/A for none)

Received Paper

TOTAL:

Number of Papers published in peer-reviewed journals:

(b) Papers published in non-peer-reviewed journals (N/A for none)

Received Paper

TOTAL:

Number of Papers published in non peer-reviewed journals:

(c) Presentations

Number of Presentations: 0.00

Non Peer-Reviewed Conference Proceeding publications (other than abstracts):

Received Paper

TOTAL:

Number of Non Peer-Reviewed Conference Proceeding publications (other than abstracts):

Peer-Reviewed Conference Proceeding publications (other than abstracts):

Received Paper

TOTAL:

Number of Peer-Reviewed Conference Proceeding publications (other than abstracts):

(d) Manuscripts

Received Paper

TOTAL:

Number of Manuscripts:

Books

Received Book

TOTAL:

Received Book Chapter

TOTAL:

Patents Submitted

Patents Awarded

Awards

Fellow of Institute of Physics (IOP) (UK)(2013)

Fellow of the American Association for the Advancement of Science (AAAS) “for distinguished contributions in the field of reaction dynamics, particularly for understanding formation mechanisms of complex molecules in extraterrestrial environments and in combustion systems”. (2013)

Graduate Students

NAME	PERCENT_SUPPORTED	Discipline
Matthew Abplanalp	0.00	
FTE Equivalent:	**0.00**	
Total Number:	**1**	

Names of Post Doctorates

NAME	PERCENT_SUPPORTED
Lloyd G Muzangwa	1.00
FTE Equivalent:	**1.00**
Total Number:	**1**

Names of Faculty Supported

NAME	PERCENT_SUPPORTED	National Academy Member
Ralf I. Kaiser	0.08	
FTE Equivalent:	**0.08**	
Total Number:	**1**	

Names of Under Graduate students supported

NAME	PERCENT_SUPPORTED
FTE Equivalent:	
Total Number:	

Student Metrics

This section only applies to graduating undergraduates supported by this agreement in this reporting period

The number of undergraduates funded by this agreement who graduated during this period: 0.00

The number of undergraduates funded by this agreement who graduated during this period with a degree in science, mathematics, engineering, or technology fields:..... 0.00

The number of undergraduates funded by your agreement who graduated during this period and will continue to pursue a graduate or Ph.D. degree in science, mathematics, engineering, or technology fields:..... 0.00

Number of graduating undergraduates who achieved a 3.5 GPA to 4.0 (4.0 max scale):..... 0.00

Number of graduating undergraduates funded by a DoD funded Center of Excellence grant for Education, Research and Engineering:..... 0.00

The number of undergraduates funded by your agreement who graduated during this period and intend to work for the Department of Defense 0.00

The number of undergraduates funded by your agreement who graduated during this period and will receive scholarships or fellowships for further studies in science, mathematics, engineering or technology fields:..... 0.00

Names of Personnel receiving masters degrees

NAME
Total Number:

Names of personnel receiving PHDs

NAME
Total Number:

Names of other research staff

NAME	PERCENT_SUPPORTED
Brant M. Jones	0.16
FTE Equivalent:	**0.16**
Total Number:	**1**

Sub Contractors (DD882)

Inventions (DD882)

1. Program Scope

The main objectives of our project within the framework of the STIR program is to understand the hitherto poorly characterized underlying reaction mechanisms involved in the explosive decomposition of model compounds of energetic materials in the condensed phase. This is aimed to change our understanding of their long-term stability and explosion efficiency and may also lead to the development of novel insensitive energetic materials. These studies involve a reaction class which has been largely overlooked by experimentalists and theoreticians for the last decades: the decomposition of model compounds of nitrohydrocarbon-, nitramine-, and nitro-ester-based energetic materials.

We trigger the decomposition of the model compounds in the solid state by ionizing radiation in form of energetic electrons and tunable UVVUV photons with energies below the ionization energy of the target molecules in a contamination free ultra high vacuum setup at low temperatures. An investigation of these processes allows a study of the temperature dependence of these processes such as branching ratios, diffusion limited mechanisms, radical-radical recombination processes, and isotopic effects. The decomposition processes are monitored on line and in situ via an array of complementary spectroscopic tools. Based on the kinetic fits of the temporal evolution of newly formed species, we extract then general concepts on the reaction mechanisms, products, intermediates, and branching ratios. The detailed knowledge of the decomposition of model compounds of energetic material and of energetic material itself enhances our capability to predict the performance and long term stability of energetic materials and molecules.

2. Recent Progress

2.1. Overview

In the first months of this project, we experimentally explored the mechanisms involved in the decomposition of the key model compound of nitrohydrocarbon-based energetic material (RNO2): nitromethane (CH_3NO_2) together with the fully deuterated counterpart (CD_3NO_2) in a novel ultra high vacuum machine (Figure 1). These experiments were conducted in the condens-ed phase at temperatures as low as 5 K within thin films of about 500 nm thickness exploiting two sets of irradiation sources - energetic electrons depositing on average 8.5 ± 0.5 eV per molecule and vacuum ultraviolet photons (10.48 eV; Ly α) with energies below the ionization energy of nitromethane (11.0 ± 0.3 eV).

The decomposition of the precursor molecules (CH_3NO_2) and the successive radical reactions were traced spectroscopically via Fourier transform infrared spectroscopy (FTIR; 500 – 10,000 cm-1) in the condensed phase on line and in situ during the radiation exposure. These studies assist extracting general concepts on the reaction mechanisms, products, and intermediates in the decomposition of model systems of energetic materials and of the radical reactions involved in the solid samples. Those data further aid the fundamental understanding of low-temperature, non-equilibrium decomposition and radical reactions in the condensed phase and the inherent energy transfer processes. After the irradiation, the samples were warmed up with moderate heating rates of 1 K min-1 and the subliming molecules were detected in the gas phase via two complementary methods: i) quadrupole mass spectrometry via electron impact ionization (100 eV) of the neutral molecules and ii) fragment-free vacuum ultraviolet (VUV) photoionization of the neutral molecules at 10.49 eV coupled with a reflectron time-of-flight mass spectrometer (Re-TOF-MS).

2.2. Experimental

2.2.1. Sample Preparation and Irradiation

The experiments were carried out in a novel, contamination-free ultra-high vacuum (UHV) chamber(Figure 1A and 1B). The main chamber is evacuated down to a base pressure typically of a few 10-11 torr using oil-free magnetically suspended turbomolecular pumps backed with dry scroll pumps. A cold finger assembled from oxygen free high conductivity copper (OFHC) is coupled to an UHV compatible closed-cycle helium refrigerator (Sumitomo Heavy Industries, RDK-415E). A polished silver mirror is then mounted to the cold finger insulated with 0.1 mm thick indium foil to ensure thermal conductivity and subsequently cooled to a final temperature of 5.5 ± 0.1 K; the entire ensemble is freely rotatable within the horizontal center plane and translatable in the vertical (z-axis) via an UHV compatible bellow and differential pumped rotational feed through. From here, the corresponding gases (CH_3NO_2, CD_3NO_2) were then deposited through a glass capillary yielding ice samples with final thicknesses of 510 ± 10 nm. The thickness of the sample was determined in situ using laser interferometry. Here, the cooled silver target is rotated to face a HeNe laser (632 nm), which strikes the target at an incident angle of 4° relative to the sample normal and reflected toward a photodiode equipped with a 632.8 nm narrow band pass filter. The induced current in the photodiode is monitored as a function of time with a picoammeter, while the gas is introduced into the chamber at a constant rate through a precision leak valve where upon it is finally condensed onto the low temperature silver target. During the deposition, the HeNe laser is reflected off the surface of silver target and the freshly deposited ice sample causing an interference pattern. The relation between the period of the interference curve between two maxima or minima relates to a change in thickness, Δd, by the equation (1), where λ0 is the laser wavelength (632.8 nm), is the incident angle (4°), and nf is the refractive index of the ice. Each of the ices was irradiated with 5 keV electrons isothermally at 5.5 ± 0.1 K for one hour at 30 nA over a square area of 1.0 ± 0.1 cm^2 and an angle of 70º relative to the surface normal. The emission current was measured prior to irradiation on line and in situ utilizing a Faraday cup mounted inside a differentially pumped chamber on an ultrahigh vacuum compatible translation state. The total dose deposited into the ice sample was determined from Monte Carlo simulations (CASINO)57 taking into consideration the scattering coefficient and the energy deposited from

the back scattered electrons. The total energy deposited into the amorphous ice was about 8.5 ± 0.5 eV per molecule. For the on line and in situ identification of new molecular band carriers of the ices during irradiation, a Fourier transform infrared spectrometer (Nicolet 6700) monitored the samples throughout the duration of the experiment with an IR spectrum collected every two minutes in the range of 6000 – 400 cm-1 at a resolution of 4 cm-1. Each FTIR spectrum was recorded in absorption–reflection–absorption mode (reflection angle = 45°) for two minutes resulting in a set of 30 infrared spectra during the radiation exposure for each system. We recognize that integrated band areas can be altered by optical interference effects inherit in absorption- reflection absorption FTIR spectroscopy; however, this issue is circumvented as shown in our group by integration of weak bands, whose absorbance remains linear with respect to the amount of ice deposited. After the irradiation, the sample was kept at 5.5 K for one hour; then, temperature programed desorption (TPD) studies were conducted by heating the irradiated ices at a rate of 0.5 K min-1 to 300 K. Throughout the thermal sublimation process, the ice samples were monitored via infrared spectroscopy and single photon ionization reflectron time-of-flight mass spectroscopy separately, i.e. each experiment was conducted twice. For the gas phase detection, the products were ionized upon sublimation via single photon ionization exploiting pulsed (30 Hz) coherent vacuum ultraviolet (VUV) light at 118.2 nm (10.49 eV) generated via non-linear four wave mixing. The ions were then extracted into a reflectron time-of-flight mass spectrometer whereupon the ions are mass resolved according to their arrival times.

2.2.2. Time-of-Flight

The reflectron time-of-flight spectrometer was used to monitor the arrival times of the products as they sublimate into the gas phase. Typically, ions are extracted into the focusing region with a repeller plate (positive voltage) and an extraction plate (negative voltage). Here, the silver target represents the repeller plate. However, as the silver target is directly mounted to the copper cold finger with indium foil to ensure thermal conductivity, no voltage can be applied to the silver target without floating the entire chamber as they have a common ground. An initial attempt was made at coupling the substrate to the cold finger utilizing a thin sapphire crystal to electorally isolate the substrate and consequently float at a small positive voltage. However, the nonlinear thermal conductivity of sapphire at cryogenic temperatures resulted in spurious and inconsistent thermal desorption profiles in the temperature regime from 5 K to 40 K. To overcome this, the field between the repeller and extractor plate was simply held at an overall negative potential. Once the molecules sublimate into the gas phase, they are then ionized by the VUV light source (10.49 eV) and then resolved by mass to charge ratio utilizing reflectron time-of-flight mass spectrometry. The ions are detected utilized a multichannel plate with a dual chevron configura-tion. From the here the signals were amplified using a fast preamplifier and shaped with a 100 MHz discriminator. The TOF spectra were recorded with a personal computer based multichan-nel scaler using a bin width of 4 ns.

3. Results

3.1. Infrared Spectroscopy (Qualitative Information)

Upon radiation exposure of the (D3)-nitromethane samples with energetic electrons, multiple new absorption features of four discrete molecules emerged (Table 1; Figure 2). Most important, the formation of methylnitrite (CH3NO2) – the structural isomer of nitromethane (CH3NO2) – was confirmed via the detection of at least four absorptions at 3196 cm-1 (2v3), 1614 cm-1 (v3), 1230/1239 cm-1 (v6), 1161 cm-1 (v13, and 835 cm-1 (v8). These positions agree nicely with those data reported previously. Further, the formaldehyde molecule (H2CO) was detected at 1720/1721 cm-1 (v2) and 1502/1499 cm-1 (v3). Finally, two simple nitrogen-bearing molecules (NO and HNO) could be sampled via their absorptions at 1876/1873 cm-1 (v1) as well as 1504 cm-1 (v3), 1468 cm-1 (v1), 991/993 cm-1 (v2), and 835 cm-1 (v8). The assignments of the absorptions were confirmed via their deuterium isotopic shifts as compiled in Table 1. It is important to stress that we did not see any absorptions of the methyl radical (CH3), nitrogen dioxide (NO2), ethane (C2H6), or dinitrogentetraoxide (N2O4), although they should not be obscured by absorptions of the parents.

3.2. Infrared Spectroscopy (Quantitative & Mechanistical Information)

Having assigned four newly formed molecules in irradiated (D3)-nitromethane ice films (CH3ONO, H2CO, NO, HNO) on line and in situ, we are now elucidating the underlying formation pathways. For this, we traced the temporal profiles of the bands during the irradiation (Figure 3) and utilized a set of coupled differential equations to numerically fit these temporal profiles. The resulting rate constants are listed in Table 2.

First, the temporal profiles and the kinetic fits suggest (pseudo) first order kinetics of the formation of methyl nitrite (CH3ONO) via isomerization of nitromethane (CH3NO2) (k1). It should be highlighted that the isomerization of D3-nitromethane is surprisingly faster than of nitromethane with k1(CD3NO2)/k1(CH3NO2) = 2.0 ± 0.8. No evidence of a unimolecular decomposition of nitromethane (CH3NO2) leading to free methyl radical (CH3) and nitrogen dioxide (NO2) was observed. Therefore, the nitromethane – methyl nitrite isomerization represents the exclusive, initial reaction step in this system.
Second, our studies proposed two competing pathways of the decomposition of methyl nitrite (CH3ONO) into formaldehyde (H2CO) plus nitrosyl hydride (HNO) and the methoxy radical (CH3O) plus nitrogen monoxide (NO) with rate constants k2 and k3, respectively. The fits propose that both in the nitromethane and D3-nitromethane systems, the molecular product channel (k2) dominates with branching ratios of (3.0±0.8) : 1 and (5.0±1.5) : 1, respectively.
Finally, to adequately fit the column densities of methyl nitrite (CH3ONO), it was important to add a back-reaction of

formaldehyde (H2CO) and nitrosyl hydride (HNO) within the matrix cage (k4). Quantitatively spoken, both nitromethane and D3-nitromethane systems hold identical equilibrium constants K (5 K) = k4/k3 of 0.3 ± 0.2 and 0.3 ± 0.1, respectively.

4.1. Mass Spectroscopy

Reflectron time-of-flight mass spectroscopy coupled to single photon ionization ('soft photoioni-zation') (ReTOF-PI) upon sublimation of the irradiated ices presents a unique advantage compared to traditional mass spectroscopy coupled with electron impact ionization at, for instance, 100 eV ('hard ionization). In principle, any molecule can be ionized by electron impact. Traditionally, the ionization of neutral molecules is conducted at electron energies between typically 80 eV and 100 eV (hard electron impact ionization), i.e. the range where the ionization cross section of organic molecules is at the maximum. However, at these electron energies, molecules undergo extensive dissociative ionization yielding significant fragment ions. In the extreme case, this can even result in a situation in which the parent ion depicts only a few percent of the total ion count or is even unstable (no signal count for the parent ion).
On the other hand, soft ionization exploiting tunable, fragment-free vacuum ultraviolet (VUV) single photon ionization can eliminate the problem of dissociative ionization and the interfering species. In most of the cases VUV photoionization only results in the formation of parent ion of the product molecule without forming fragment ions thus essentially eliminating dissociative ionization. Most importantly, by selectively tuning the ionization energy above the ionization energy of one molecule, but below the ionization energy of a second molecule, isomers can be ionized selectively.
This is of particular relevance to the present system. After the electron exposure of the icy films, the irradiated (D3)-nitromethane samples are warmed up with 0.5 K min-1 to 300 K. As pictured in Figure 1B, the photoionization laser (10.49 eV) interrogates the subliming molecules almost perpendicularly above the silver target. The resulting ion currents as a function of temperature and mass-to-charge are compiled for all systems in Figure 5. Here, the subliming nitromethane (CH3NO2) cannot be photoionized since its ionization energy (11.08 eV) is above the energy of the photoionization laser. On the other hand, the methylnitrite (CH3ONO), which presents the isomerization product of nitromethane, holds an ionization energy of only 10.44 eV and can be photoionized. Therefore, ion signal at mass-to-charge of 61 can only originate from CH3ONO+, but not from CH3NO2+ (Table 3).
The individual TOF spectra are compiled in Figure 6 with masses listed and cross linked to their deuterated counterparts in Table 3. Nitrogen monoxide could be identified via its parent ion in all systems at m/z = 30. Nitrosyl hydride (HNO) and its deuterated counterpart could be probed at m/z = 31 (HNO+) and 32 (DNO+), respectively. The methylnitrite isomer (CH3ONO) and its 13C substituted counterpart (13CH3ONO) were detected at m/z = 61 and 62, respectively. The shift by three amu in the D3-nitromethane sample rises to ion counts at m/z = 64 and 65 for CH3ONO and 13CH3ONO, respectively. Note that the ionization energy of formaldehyde (H2CO; 10.88 eV) is above the energy of the ionization laser. However, the appearance of additional ion peaks with up to 75 amu, which cannot be linked to the infrared spectroscopically derived reaction pathways as compiled in Figure 4, clearly indica-tes a more complex chemistry in the condensed phase than previously thought. The data analysis of these TOFs is still ongoing, so only a preliminary analysis is given here. First, the TOFs at m/z = 33 (H2NOH+) and 36 (D2NOD+) propose the existence of free (suprathermal) hydrogen atoms, which can hydrogen atoms which can hydrogenate the nitrosyl hydride molecule (HNO). Second, the detection of signal at m/z = 45 and the corresponding shift to m/z = 48 indicated a system with three hydrogen atoms, i.e. H2CNOH and/or CH3NO. The latter might be formed as a minor product via recombination of nitrogen monoxide (NO) with methyl radicals (CH3) present in the ices below the infrared spectroscopic detection limit. Finally, signal at m/z = 47 – shifted to 52 upon deuteration by 5 amu – clearly proposed a molecule carrying five hydrogen atoms, i.e. CH3NHOH and CD3NDOD. Reaction pathways to this molecule are still under consideration, but they are expected to involve higher order reaction steps.

4. Summary

We presented a preliminary data analysis of the electron-induced decomposition of nitromethane (CH3NO2) in the condensed phase at 5 K. The following findings shall be highlighted.

1. Infrared spectroscopically, we have identified four newly formed molecules in irradiated (D3)-nitromethane ice films: CH3ONO, H2CO, NO, and HNO.

2. We also elucidated the underlying formation pathways by tracing the temporal profiles of the bands during the irradiation and numerically fitting these temporal profiles.

3. The data analysis suggest (pseudo) first order kinetics of the formation of methyl nitrite (CH3ONO) via isomerization of nitromethane (CH3NO2) (k1) in the condensed phase. In the gas phase, this pathway has been proposed to involve a roaming-mediated isomerization via an initial carbon-nitrogen bond rupture. However, in the condensed phase, both the methyl radical and the nitrogen dioxide formed via the carbon-nitrogen bond rupture are trapped within the matrix cage and can recombine back either to nitromethane (CH3NO2) or methyl nitrite (CH3ONO). In the condensed phase, roaming reaction dynamics are not required to explain the experimental data. The isomerization of D3-nitromethane is surprisingly faster than of nitromethane with k1(CD3NO2)/k1(CH3NO2) = 2.0 ± 0.8. This proposed non-equilibrium reaction dynamics in the condensed phase. This 'cage effect' is reflected in reaction mechanisms, which do not exist in gas phase reactions under single collision conditions, where the nascent products 'fly apart' or undergo prior reactions via 'roaming'.

4. No evidence of a unimolecular decomposition of nitromethane (CH3NO2) leading to free methyl radical (CH3) and nitrogen dioxide (NO2) was observed. Therefore, the nitromethane – methyl nitrite isomerization represents the exclusive, initial reaction step in this system. This is in strong discrepancy to the unimolecular decomposition of nitromethane in the gas phase, where the carbon-nitrogen bond is split, and the methyl radical (CH3) and nitrogen dioxide (NO2) products fly apart undisturbed. Infrared multi photon (IRMPD) and ultraviolet photodissociation (UVPD) of nitromethane (CH3NO2) have been exploited for years. In a pioneering molecular beams experiment by Lee et al., infrared multi photon dissociation studies utilizing the 10.6 μm output of a carbon dioxide laser suggested the existence of two processes via carbon-nitrogen and oxygen-nitrogen bond cleavage processes, i.e. the channels CH3 + NO2 and CH3O + NO with the latter being dominant involving the methyl nitrite isomer (CH3ONO). Follow up experiments at 193 nm indicated that the cleavage of the carbon-nitrogen bond and production of the methyl radical (CH3) plus nitrogen dioxide (NO2) was the primary process. In the condensed phase, however, the initial fragments are hindered by the matrix cage and hence react back either to nitromethane (CH3NO2) or isomerize to methyl nitrite (CH3ONO).

5. Methyl nitrite (CH3ONO) was found to decompose via two competing pathways into formaldehyde (H2CO) plus nitrosyl hydride (HNO) and the methoxy radical (CH3O) plus nitrogen monoxide (NO) with rate constants k2 and k3, respectively. The fits propose that both in the nitromethane and D3-nitromethane systems, the molecular product channel (k2) dominates with branching ratios of (3.0±0.8) : 1 and (5.0±1.5) : 1, respectively. The dominance of the molecular product channel is quite distinct from the gas phase experiments depicting a prevailing radical channel (Bowen et al. JPCA 117, 11665-11672).

6. Reflectron time-of-flight mass spectroscopy coupled to single photon ionization (‘soft photo-ionization’) (ReTOF-PI) revealed that the reaction mechanisms in the condensed phase are more complex than in the gas phase. These involve, for instance, addition of suprathermal hydrogen atoms (leading eventually to H2NOH), radical-radical recombination reactions (CH3NO), and hitherto poorly elucidated pathways leading to hydroxymethylamine (CH3NHOH). Reaction pathways to this molecule are still under consideration, but they are expected to involve higher order reaction steps reflecting that the decomposition of energetic materials and their model compounds in the solid state is more complex and can yield to a greater variety of reaction inter-mediates, products, and reaction mechanisms compared to the analog processes in the gas phase under collision-less conditions, where the primary products can fly undisturbed to the detector.

5. Future Plans

We are planning to expand the research on the following levels:

L1: To finalize the data analysis of the electron induced decomposition of (D3) nitromethane (CH3NO2) in the condensed phase and to disseminate the results.
L2: To start the data analysis of Lyman α (10.49 eV) photolyzed (D3) nitromethane (CH3NO2) ice films.
L3: To engage a collaboration with Joel Bowman (Emory) on the Lyman α experiments and to compare our experimental branching ratios with those obtained from calculations on photolyzed nitromethane clusters.

Technology Transfer

Untangling the Reaction Mechanisms Involved in the Explosive Decomposition of Model Compounds of Energetic Materials

Principal Investigator: Ralf I. Kaiser

Department of Chemistry, University of Hawaii at Manoa, Honolulu, HI 06822

ralfk@hawaii.edu

Program Manager: James K. Parker

Physical and Theoretical Chemistry, Chemical Sciences Division, U.S. Army Research Office
P.O. Box 12211, Research Triangle Park NC 27709

james.kenneth.parker@us.army.mil;baa@arl.army.mil

Final Report

1. Program Scope

The main objectives of our project within the framework of the STIR program is to understand the hitherto poorly characterized underlying reaction mechanisms involved in the explosive decomposition of model compounds of energetic materials in the condensed phase. This is aimed to change our understanding of their long-term stability and explosion efficiency and may also lead to the development of novel insensitive energetic materials. These studies involve a reaction class which has been largely overlooked by experimentalists and theoreticians for the last decades: the decomposition of model compounds of nitrohydrocarbon-, nitramine-, and nitroester-based energetic materials.

We trigger the decomposition of the model compounds in the solid state by ionizing radiation in form of energetic electrons and tunable UVVUV photons with energies below the ionization energy of the target molecules in a contamination free ultra high vacuum setup at low temperatures. An investigation of these processes allows a study of the temperature dependence of these processes such as branching ratios, diffusion limited mechanisms, radical-radical recombination processes, and isotopic effects. The decomposition processes are monitored *on line* and *in situ* via an array of complementary spectroscopic tools. Based on the kinetic fits of the temporal evolution of newly formed species, we extract then general concepts on the reaction mechanisms, products, intermediates, and branching ratios. The detailed knowledge of the decomposition of model compounds of energetic material and of energetic material itself enhances our capability to predict the performance and long term stability of energetic materials and molecules.

2. Recent Progress

2.1. Overview

In the first months of this project, we experimentally explored the mechanisms involved in the decomposition of *the* key model compound of nitrohydrocarbon-based energetic material (RNO_2): nitromethane (CH_3NO_2) together with the fully deuterated counterpart (CD_3NO_2) in a novel ultra high vacuum machine (Figure 1). These experiments were conducted in the condensed phase at temperatures as low as 5 K within thin films of about 500 nm thickness exploiting two sets of irradiation sources - energetic electrons depositing on average 8.5 ± 0.5 eV per molecule and vacuum ultraviolet photons (10.48 eV; Ly α) with energies below the ionization energy of nitromethane (11.0 ± 0.3 eV).

The decomposition of the precursor molecules (CH_3NO_2) and the successive radical reactions were traced spectroscopically via Fourier transform infrared spectroscopy (FTIR; 500 – 10,000 cm^{-1}) in the condensed phase *on line* and *in situ* during the radiation exposure. These studies assist extracting general concepts on the reaction mechanisms, products, and intermediates in the decomposition of model systems of energetic materials and of the radical reactions involved in the solid samples. Those data further aid the fundamental understanding of low-temperature, non-equilibrium decomposition and radical reactions in the condensed phase and the inherent energy transfer processes. After the irradiation, the samples were warmed up with moderate heating rates of 1 K min^{-1} and the subliming molecules were detected in the gas phase via two complementary methods: i) quadrupole mass spectrometry via electron impact ionization (100 eV) of the neutral molecules and ii) fragment-free vacuum ultraviolet (VUV) photoionization of the neutral molecules at 10.49 eV coupled with a reflectron time-of-flight mass spectrometer (Re-TOF-MS).

2.2. Experimental

2.2.1. Sample Preparation and Irradiation

The experiments were carried out in a novel, contamination-free ultra-high vacuum (UHV) chamber (Figure 1A and 1B). The main chamber is evacuated down to a base pressure typically of a few 10^{-11} torr using oil-free magnetically suspended turbomolecular pumps backed with dry scroll pumps. A cold finger assembled from oxygen free high conductivity copper (OFHC) is coupled to an UHV compatible closed-cycle helium refrigerator (Sumitomo Heavy Industries, RDK-415E). A polished silver mirror is then mounted to the cold finger insulated with 0.1 mm thick indium foil to ensure thermal conductivity and subsequently cooled to a final temperature of 5.5 ± 0.1 K; the entire ensemble is freely rotatable within the horizontal center plane and translatable in the vertical (z-axis) via an UHV compatible bellow and differential pumped rotational feed through. From here, the corresponding gases (CH_3NO_2, CD_3NO_2) were then deposited through a glass capillary yielding ice samples with final thicknesses of 510 ± 10 nm The thickness of the sample was determined *in situ* using laser interferometry. Here, the cooled silver target is rotated to face a HeNe laser (632 nm), which strikes the target at an incident angle of 4° relative to the sample normal and reflected toward a photodiode equipped with a 632.8 nm narrow band pass filter. The induced current in the photodiode is monitored as a function of time with a picoammeter, while the gas is introduced into the chamber at a constant rate through a precision leak valve where upon it is finally condensed onto the low temperature silver target. During the deposition, the HeNe laser is reflected off the surface of silver target and the freshly deposited ice sample causing an interference pattern. The relation between the period of the interference curve between two maxima or minima relates to a change in thickness, Δd, by the equation (1), where λ_0 is the laser wavelength (632.8 nm), θ_i is the incident angle (4°), and n_f is the refractive index of the ice.

(1)
$$\Delta d = \frac{\lambda_0}{2n_f\sqrt{1-sin^2\theta_i/n_f^2}}$$

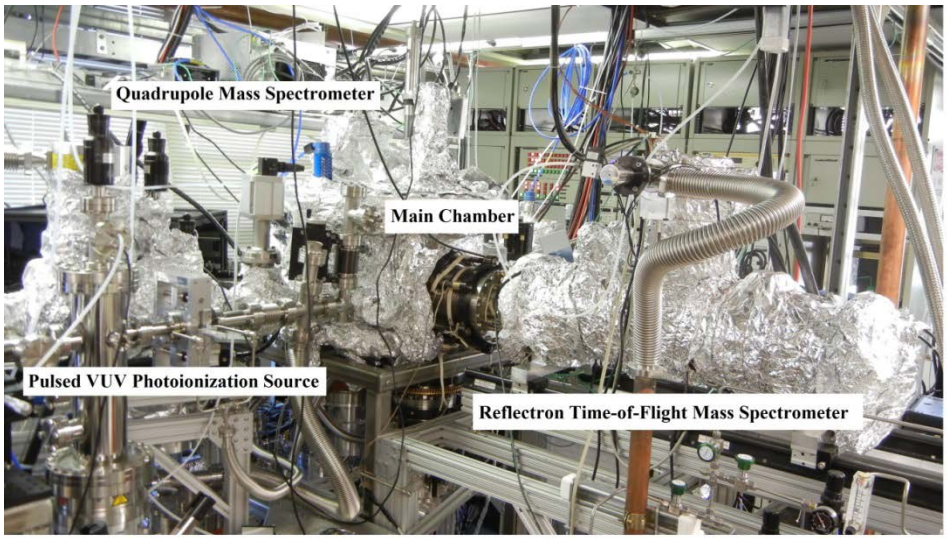

Figure 1A. Front view of the experimental setup.

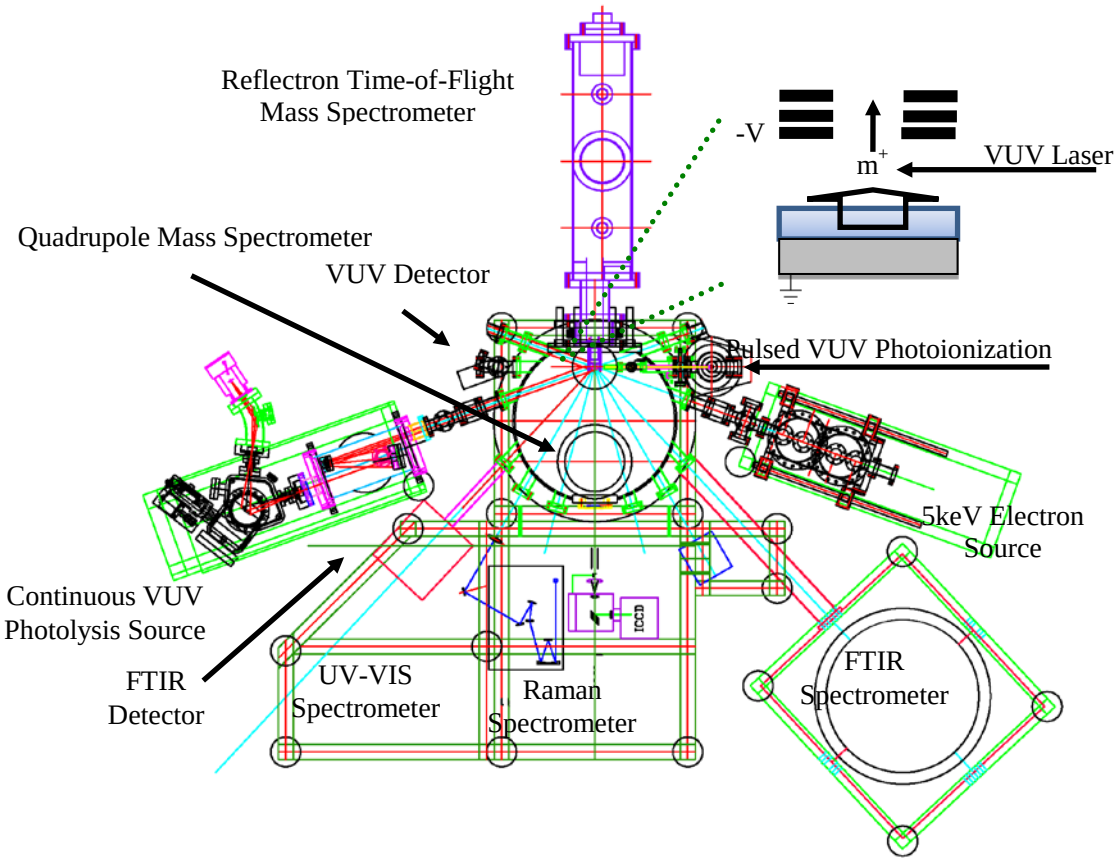

Figure 1B. Schematic top view of the main chamber including the analytical instruments, radiation sources, and the cryogenic target (point of converging lines). The alignment of the cryogenic target, radiation sources, and infrared, spectrometer allows simultaneous on line and *in situ* measurements of the modification of the targets upon the irradiation exposure. After the irradiation, the cold head can be rotated 180° to face the ReTOF mass spectrometer; the target can then be warmed up allowing the newly formed products to sublimate where upon they are photo ionized and mass analyzed. The inset (top right) shows the geometry of the ReTOF ion source lenses with respect to the target and ionization laser.

Each of the ices was irradiated with 5 keV electrons isothermally at 5.5 ± 0.1 K for one hour at 30 nA over a square area of 1.0 ± 0.1 cm^2 and an angle of 70º relative to the surface normal. The emission current was measured prior to irradiation on line and in situ utilizing a Faraday cup mounted inside a differentially pumped chamber on an ultrahigh vacuum compatible translation state. The total dose deposited into the ice sample was determined from Monte Carlo simulations (CASINO)[57] taking into consideration the scattering coefficient and the energy deposited from the back scattered electrons. The total energy deposited into the amorphous ice was about 8.5 ± 0.5 eV per molecule.

For the *on line* and *in situ* identification of new molecular band carriers of the ices during irradiation, a Fourier transform infrared spectrometer (Nicolet 6700) monitored the samples throughout the duration of the experiment with an IR spectrum collected every two minutes in the range of 6000 – 400 cm^{-1} at a resolution of 4 cm^{-1}. Each FTIR spectrum was recorded in absorption–reflection–absorption mode (reflection angle = 45°) for two minutes resulting in a set of 30 infrared spectra during the radiation exposure for each system. We recognize that integrated band areas can be altered by optical interference effects inherit in absorption-reflection-

2.2.2. VUV Generation

Pulsed coherent vacuum ultraviolet (VUV) light at 118.2 nm (10.49 eV) was generated exploiting a nonlinear four wave mixing process ($\omega_{vuv} = 3\omega_1$) utilizing xenon as the nonlinear medium. Briefly, the mechanism behind non-linear four wave mixing is described below. The polarizability of a material in a weak electric field may be ascribed by a simple linear relationship,

(2) $$\vec{P} = \epsilon_0 \chi \vec{E}$$

However, in the presence of an intense electric field, higher order non-linear terms must be considered:

(3) $$\vec{P} = \epsilon_0 \left(\chi^{(1)} \vec{E} + \chi^{(2)} \vec{E}^2 + \chi^{(3)} \vec{E}^3 + \cdots \right)$$

If we considered a simple and very intense propagating electromagnetic wave with frequency ω_1,

(4) $$E = E_0 cos(\omega_1 t)$$

Then

(5) $$\vec{P} = \epsilon_0 \left(\chi^{(1)} E_0 cos(\omega_1 t) + \chi^{(2)} E_0 cos(\omega_1 t)^2 + \chi^{(3)} E_0 cos(\omega_1 t)^3 + \cdots \right)$$

From here, the third order cosine can be reduced using the power reducing trigonometry identity,

(6) $$cos^3(\theta) = \frac{3\cos(\theta) + \cos(3\theta)}{4}$$

giving a term in *P* as

(7) $$\frac{1}{4} \varepsilon_0 E_0 \cos(3\omega_1 t)$$

Essentially, a very intense electromagnetic field can induce an ensuing field in a medium with a non-zero third order electric susceptibility $\chi^{(3)}$ oscillating at three times the input frequency. Here, ω_1 is the third harmonic (354.6 nm) output of a high power pulsed neodymium-doped yttrium aluminum garnet laser (Nd:YAG, Spectra Physics, PRO-250) operated at 30 Hz. Typical operating values for the fundamental (ω_1) at 0.8 W or 27 mJ per pulse. The pulsed xenon gas jet was housed in a separated mixing chamber evacuated by a 400 l s^{-1} turbomolecular pump. The pulsed valve fired 286 µs prior to the Q-switch of the Nd:YAG laser. The pulsed valve was connected to the middle entrance of a T shape channel with a 1 mm diameter at 25 mm in length whereupon, xenon (Specialty Gases of America, 99.999%) from the pulsed valve entered the T shape adapter thereby forming an instantaneous pulsed mixing cell in line with the propagating ω_1 pulse. Nominal operating pressures during VUV generation are on the order of 4×10^{-4} torr with the generation chamber with the pulse valve maintained at a xenon backing pressure of 2.7 atm, derived from empirical optimization. The ω_1 laser beam was empirically focused into a T-shaped adapter on the valve to yield optimal VUV intensity.

Separation of the ω_1 fundamental (354.6 nm, 3.496 eV) from generated ω_{VUV} (118.2 nm, 10.49 eV) beam was accomplished using an off axis LiF plano-convex lens (Figure 1C). The separation lens was differentially pumped to maintain ultra-high vacuum conditions (~10^{-11} torr) within the main chamber while being coupled to the VUV mixing chamber (~10^{-4} torr). Here, the LiF lens was mounted in a flat stainless steel plate that was then sealed with two parallel plates, (with a one inch diameter hole in the center) holding concentric O-rings with different inner diameters on both sides. A small port in between the two O-rings of each plate was drilled through and coupled with corresponding vacuum fittings that allowed the evacuation via a small turbo molecular pumping station. This setup allows the lens to move horizontally in a direction that is perpendicular to the propagating ω_1 and ω_{VUV} beam axis, while constantly being evacuated to typical pressures of 10^{-8} torr. The separation lens housing was then connected to the main chamber with a port alignment flange and a standard nipple with a 0.5 cm hole drilled into a solid copper gasket evacuated by a separate turbo molecular pump with typical operating pressures of 10^{-10} torr. The solid copper gasket served two functions in that it aided in blocking out the fundamental ω_1 beam and assisted in differential pumping allowing for the maintained UHV conditions in the main chamber. In addition, the entire VUV generation chamber was rotated about 5º to compensate for the deflection angle of the lithium fluoride (LiF) separation lens for the generated VUV beam. Two detectors we used in order to monitor and optimize the generated VUV light, and to ensure proper alignment through the main chamber; these detectors operate on the photoelectric principle and were constructed of high purity OFHC copper consisting of one solid disk (diameter of 1.25 cm, thickness of 0.38 cm) coupled to a ring (inner diameter of 0.5 cm) with ceramic insulators separated by a distance of 0.2 cm. A voltage of 350 V is applied to the ring; once the VUV photons hit the solid copper disk, electrons are then ejected and collected via the ring with the supplied voltage. The pulsed voltage induced from the collected current is then monitored on digital oscilloscope with typical values at 900 mV with a 4 ns pulse width. Utilizing this information while assuming total collection efficiency with no additional secondary electrons from spurious plasma generation, we can estimate the amount of VUV photons per pulse at about 10^{14} photons per pulse.

2.2.3. Time-of-Flight

The reflectron time-of-flight spectrometer was used to monitor the arrival times of the products as they sublimate into the gas phase. Typically, ions are extracted into the focusing region with a repeller plate (positive voltage) and an extraction plate (negative voltage). Here, the silver target represents the repeller plate. However, as the silver target is directly mounted to the copper cold finger with indium foil to ensure thermal conductivity, no voltage can be applied to the silver target without floating the entire chamber as they have a common ground. An initial attempt was made at coupling the substrate to the cold finger utilizing a thin sapphire crystal to electorally isolate the substrate and consequently float at a small positive voltage. However, the nonlinear thermal conductivity of sapphire at cryogenic temperatures resulted in spurious and inconsistent thermal desorption profiles in the temperature regime from 5 K to 40 K. To overcome this, the field between the repeller and extractor plate was simply held at an overall negative potential. Once the molecules sublimate into the gas phase, they are then ionized by the VUV light source (10.49 eV) and then resolved by mass to charge ratio utilizing reflectron time-of-flight mass spectrometry. The ions are detected utilized a multichannel plate with a dual chevron configuration. From the here the signals were amplified using a fast preamplifier and shaped with a 100 MHz discriminator. The TOF spectra were recorded with a personal computer based multichannel scaler using a bin width of 4 ns.

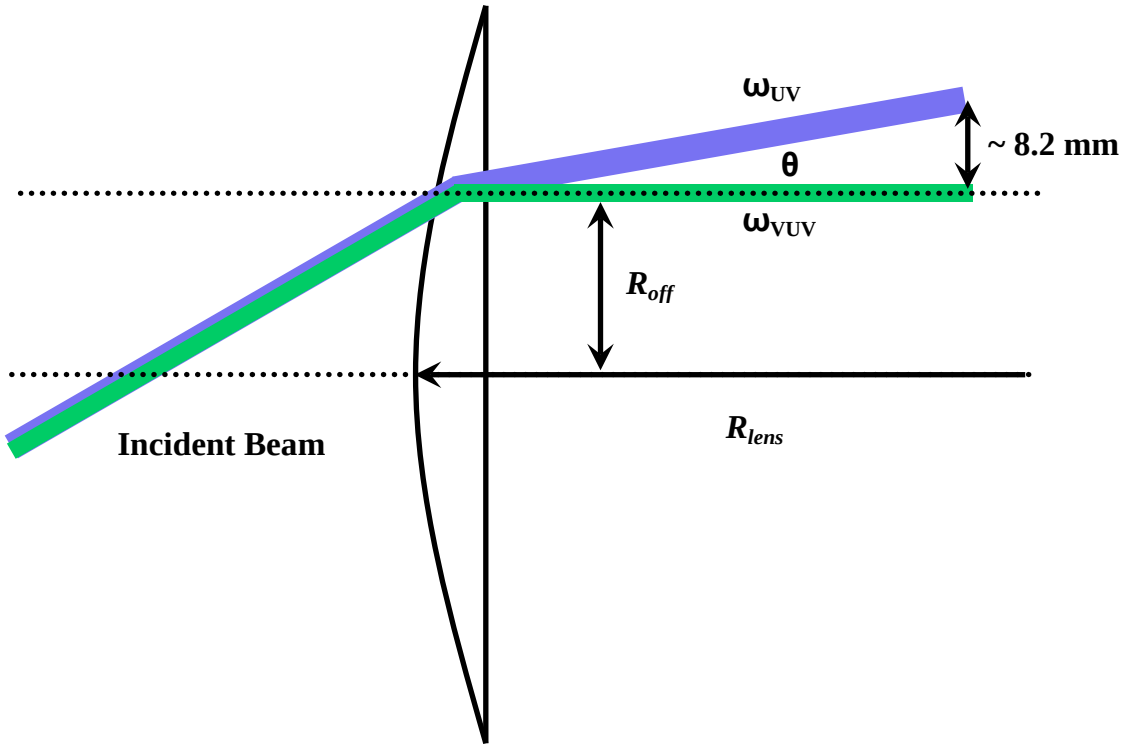

Figure 1C. Schematic representation of the separation of the two collinear ω_{UV} (blue) and ω_{VUV} (green) beams utilizing an off axis planoconvex lithium fluoride (LiF) lens. The geometry of the experimental setup allows for a separation of approximately 8.2 mm between the two beams. See text for details describing the angle of separation (θ) and associated constants; the figure is not drawn to scale for clarity.

3. Results

3.1. Infrared Spectroscopy (Qualitative Information)

Upon radiation exposure of the (D3)-nitromethane samples with energetic electrons, multiple new absorption features of four discrete molecules emerged (Table 1; Figure 2). Most important, the formation of methylnitrite (CH_3NO_2) – the structural isomer of nitromethane (CH_3NO_2) – was confirmed via the detection of at least four absorptions at 3196 cm^{-1} ($2\nu_3$), 1614 cm^{-1} (ν_3), 1230/1239 cm^{-1} (ν_6), 1161 cm^{-1} (ν_{13}, and 835 cm^{-1} (ν_8). These positions agree nicely with those data reported previously. Further, the formaldehyde molecule (H_2CO) was detected at 1720/1721 cm^{-1} (ν_2) and 1502/1499 cm^{-1} (ν_3). Finally, two simple nitrogen-bearing molecules (NO and HNO) could be sampled via their absorptions at 1876/1873 cm^{-1} (ν_1) as well as 1504 cm^{-1} (ν_3), 1468 cm^{-1} (ν_1), 991/993 cm^{-1} (ν_2), and 835 cm^{-1} (ν_8). The assignments of the absorptions were confirmed via their deuterium isotopic shifts as compiled in Table 1. It is important to stress that we did not see any absorptions of the methyl radical (CH_3), nitrogen dioxide (NO_2), ethane (C_2H_6), or dinitrogentetraoxide (N_2O_4), although they should not be obscured by absorptions of the parents.

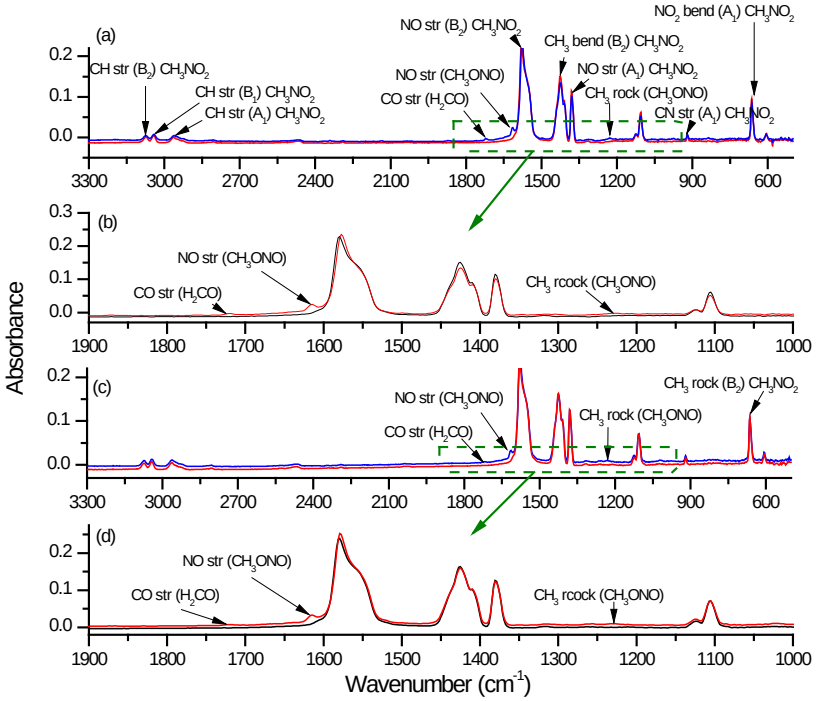

Figure 2A. Infrared spectra of the nitromethane ices at 5.5 K before (red) and after (blue) the irradiation at 100 nA ((a)/(b)) and 50 nA ((c)/(d)).

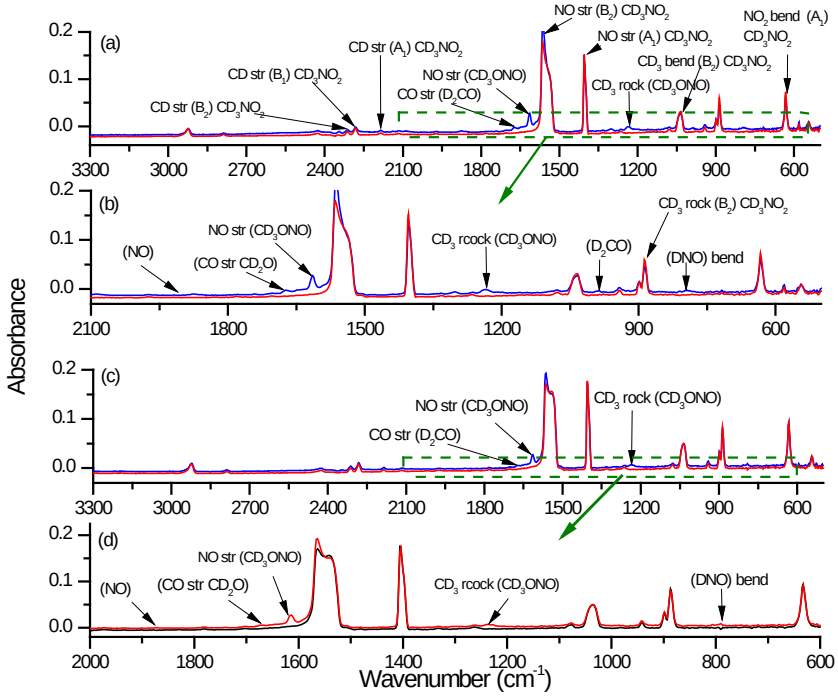

Figure 2B. Infrared spectra of the D3-nitromethane ices at 5.5 K before (red) and after (blue) the irradiation at 100 nA ((a)/(b)) and 50 nA ((c)/(d)).

CH_3NO_2			CD_3NO_2		
This Work	lit	Assignment	This Work	lit	Assignment
3074	3072	υ_1 (CH str (B_2) CH_3NO_2)	2281	2280	υ_2 (CD str (B_2) CD_3NO_2)
3041	3045	υ_1 (CH str (B_1) CH_3NO_2)	2184	2185	υ_{11} (CD str (A_1) CD_3NO_2)
2964	2958	υ_2 (CH str (A_1) CH_3NO_2)	1564	1567	υ_3 (NO str (B_2) CD_3NO_2)
1577	1571	υ_{11} (NO str (B_2) CH_3NO_2)	1403	1401	----
1425	1428	υ_4 (CH_3 bend (B_2) CH_3NO_2)	1076	1077	υ_1 (CD str (B_1) CD_3NO_2)
1380	1381	υ_5 (NO str (A_1) CH_3NO_2)	1035	1038	υ_5 (CD_3 bend (B_2) CD_3NO_2)
1124	1125	υ_6 (CH_3 rock (B_1) CH_3NO_2)	898	897	υ_6 (CD_3 rock (B_1) CD_3NO_2)
1105	1102	υ_{13} (CH_3 rock (B_2) CH_3NO_2)	632	-----	υ_8 (NO_2 bend (A_1) CD_3NO_2)
919	921	υ_7 (CN str (A_1) CH_3NO_2)	------	-----	------
663	660	υ_8 (NO_2 bend (A_1) CH_3NO_2)	------	------	------

*Verderame et al. (1972)

Table 1B. New absorption features observed in the nitromethane (CH_3NO_2) ice after irradiation.

50nA	100 nA	Lit	Assignment	Reference
----	3196	3199	$2\upsilon_3$ (N-O str; CH_3ONO)	1
----	2137	----	----	----
1873	1872	1869	υ_1 (NO)	2
1866	1872	1869	υ_1 (NO)	2
----	1759	----	----	----
----	1741	----	----	----
1721	1720	1726	υ_2 (H_2CO)	2
1614	1614	1613	υ_3 (N-O str; CH_3ONO)	1 and 5
----	1504	1505	υ_3 (HNO bend)	3 and 6
1502	1499	1498	υ_3 (H_2CO)	2
1468	----	1468	υ_1 (N-O str HNO)	4
1348	----	----	----	----
1230	1229	1230 and 1239	υ_6 (CH_3 rock CH_3ONO)	1 and 5
1165	----	1141	υ_{13} (CH_3 rock CH_3ONO)	1
993	991	992	υ_2 (HNO bend)	4
977	975	990 (broad)	υ_7 (C-O str CH_3ONO) υ_2 (HNO bend)	1 4
----	835	837 and 838	υ_8 (N-O str CH_3ONO)	1 and 5

1. The Journal of Physical Chemistry, Vol 98, No 26, 1994
2. The Journal of Chemical Pysics Vol 29, No 4, 1958
3. Jacox and Milligan, 1973 NIST website
4. Ellis and Ellison, 1983 NIST website
5. CH_3ONO NIST: http://cccbdb.nist.gov/exp2.asp
6. Johns and McKellar NIST website
7. Journal of Phys Chem, 87, 1983, 3126-3135

$_3NO_2$) ice after irradiation.

50nA	100nA	Lit	Assignment	Reference
2081	2088	2080	υ_1 (D_2CO)	2
1877	1888	----	----	----
----	1886	1883	υ_1 (NO)	3
1873	1874	1871	υ_1 (NO)	2
1741	1741	----	----	----
1673	1673	1684	υ_2 (D_2CO)	7
1614	1614		υ_3 (N-O str CD_3ONO)	
1508	1509			
1454		1452	υ_3 (N-O str DNO)	4
-----	1302			
1235	1238			
1226	1229			
----	1096			
----	992	993 and 988	υ_5 (D_2CO)	3 and 2
----	934			
----	923		υ_7 (C-O str CD_3ONO)	
806	810	822	υ_1 (DNO)	2
791	787	750±140	υ_2 (DNO bend)	NIST

1. The Journal of Physical Chemistry, Vol 98, No 26, 1994; 2. The Journal of Chemical Pysics Vol 29, No 4, 1958 3. Jacox and Milligan, 1973 NIST website; 4. Ellis and Ellison, 1983 NIST website; 5. CH_3ONO NIST: ; 6. Johns and McKellar NIST website; 7. Journal of Phys Chem, 87, 1983, 3126-3135

3.2. Infrared Spectroscopy (Quantitative & Mechanistical Information)

Having assigned four newly formed molecules in irradiated (D3)-nitromethane ice films (CH_3ONO, H_2CO, NO, HNO) on line and in situ, we are now elucidating the underlying formation pathways. For this, we traced the temporal profiles of the bands during the irradiation (Figure 3) and utilized a set of coupled differential equations to numerically fit these temporal profiles. The resulting rate constants are listed in Table 2.

First, the temporal profiles and the kinetic fits suggest (pseudo) first order kinetics of the formation of methyl nitrite (CH_3ONO) via isomerization of nitromethane (CH_3NO_2) (k_1). It should be highlighted that the isomerization of D3-nitromethane is surprisingly faster than of nitromethane with $k_1(CD_3NO_2)/k_1(CH_3NO_2) = 2.0 \pm 0.8$. No evidence of a unimolecular decomposition of nitromethane (CH_3NO_2) leading to free methyl radical (CH_3) and nitrogen dioxide (NO_2) was observed. Therefore, the nitromethane – methyl nitrite isomerization represents the exclusive, initial reaction step in this system.

Second, our studies proposed two competing pathways of the decomposition of methyl nitrite (CH_3ONO) into formaldehyde (H_2CO) plus nitrosyl hydride (HNO) and the methoxy radical (CH_3O) plus nitrogen monoxide (NO) with rate constants k_2 and k_3, respectively. The fits propose that both in the nitromethane and D3-nitromethane systems, the molecular product channel (k_2) dominates with branching ratios of (3.0±0.8) : 1 and (5.0±1.5) : 1, respectively.

Finally, to adequately fit the column densities of methyl nitrite (CH_3ONO), it was important to add a back-reaction of formaldehyde (H_2CO) and nitrosyl hydride (HNO) within the matrix cage (k_4). Quantitatively spoken, both nitromethane and D3-nitromethane systems hold identical equilibrium constants K (5 K) = k_4/k_3 of 0.3 ± 0.2 and 0.3 ± 0.1, respectively.

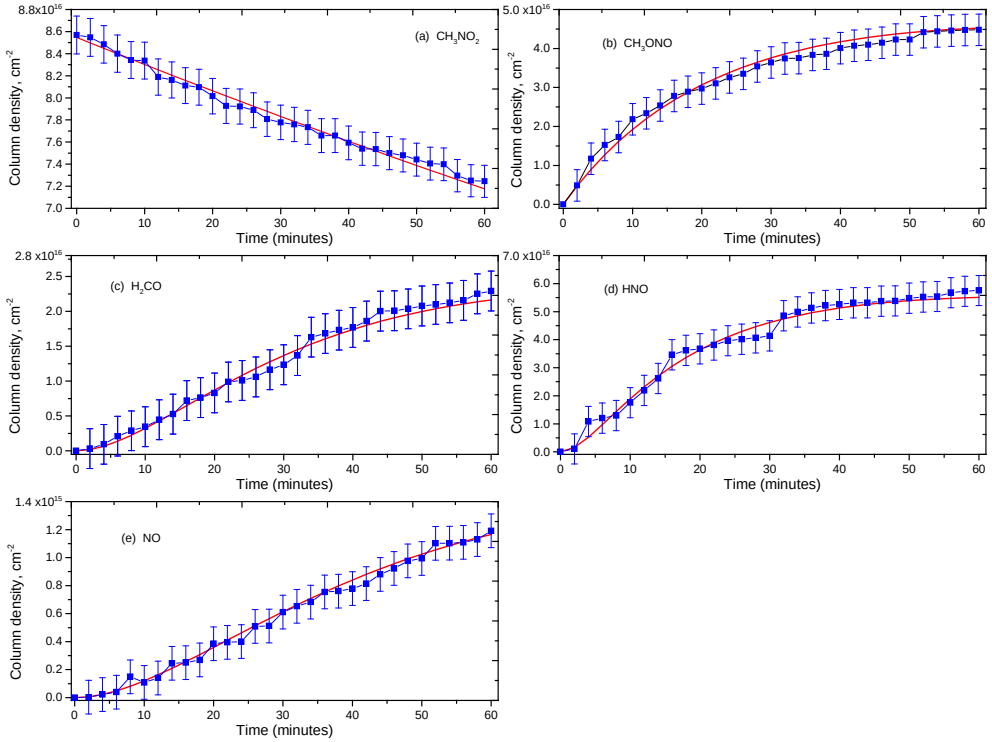

Figure 3A. Fits of the temporal profile of the absorption peak at 1380 cm^{-1} (parent (a)) and of the products at 1614 cm^{-1} (b), 1720 cm^{-1} (c), 975 cm^{-1} (d), and 1872 cm^{-1} (e) during the irradiation of nitromethane ice.

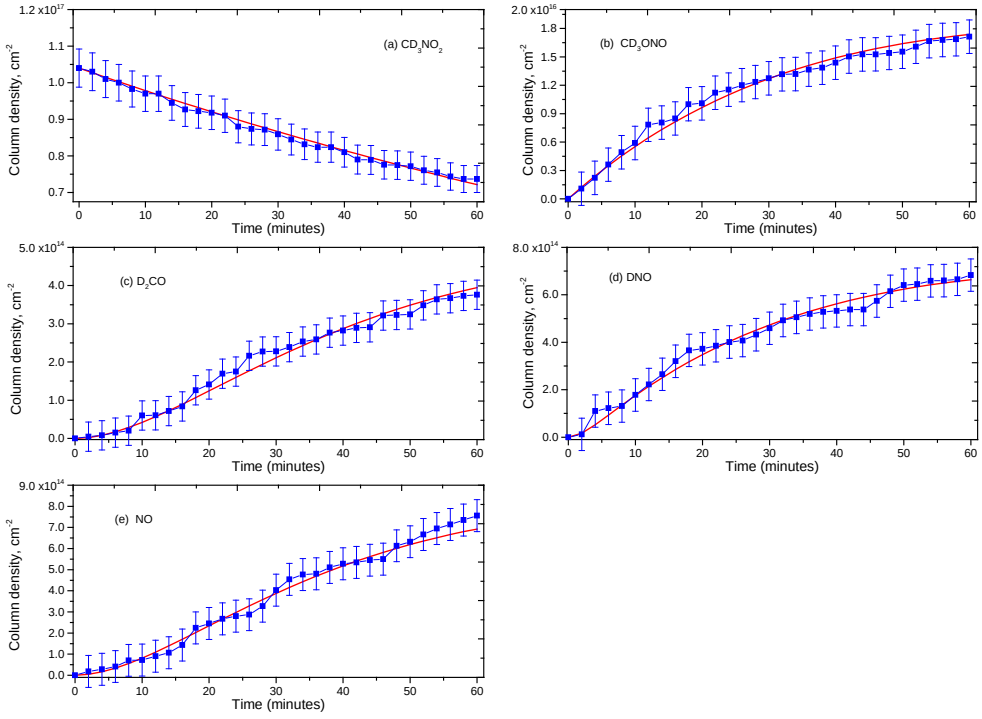

Figure 3B. Fits of the temporal profile of the absorption peak at 1380 cm^{-1} (parent (a)) and of the products at 1614 cm^{-1} (b), 1672 cm^{-1} (c), 1454 cm^{-1} (d), and 1873 cm^{-1} (e) during the irradiation of nitromethane ice.

Table 2. Rate constants derived via iterative solution of the reaction scheme depicted in Figure 4.

Reaction	Rate Constant (s^{-1})
$CH_3NO_2 \longrightarrow CH_3ONO$	$k_1 = (0.5 \pm 0.1) \times 10^{-4}$
$CH_3ONO \longrightarrow H_2CO + HNO$	$k_2 = (6.6 \pm 0.2) \times 10^{-4}$
$CH_3ONO \longrightarrow H_3CO + NO$	$k_3 = (2.2 \pm 0.5) \times 10^{-4}$
$H_2CO + HNO \longrightarrow CH_3ONO$	$k_4 = (0.7 \pm 0.1) \times 10^{-4}$

Reaction	Rate Constant (s^{-1})
$CD_3NO_2 \longrightarrow CD_3ONO$	$k_1 = (1.0 \pm 0.2) \times 10^{-4}$
$CD_3ONO \longrightarrow D_2CO + DNO$	$k_2 = (3.0 \pm 0.4) \times 10^{-4}$
$CD_3ONO \longrightarrow D_3CO + NO$	$k_3 = (0.6 \pm 0.1) \times 10^{-4}$
$D_2CO + DNO \longrightarrow CD_3ONO$	$k_4 = (0.2 \pm 0.1) \times 10^{-4}$

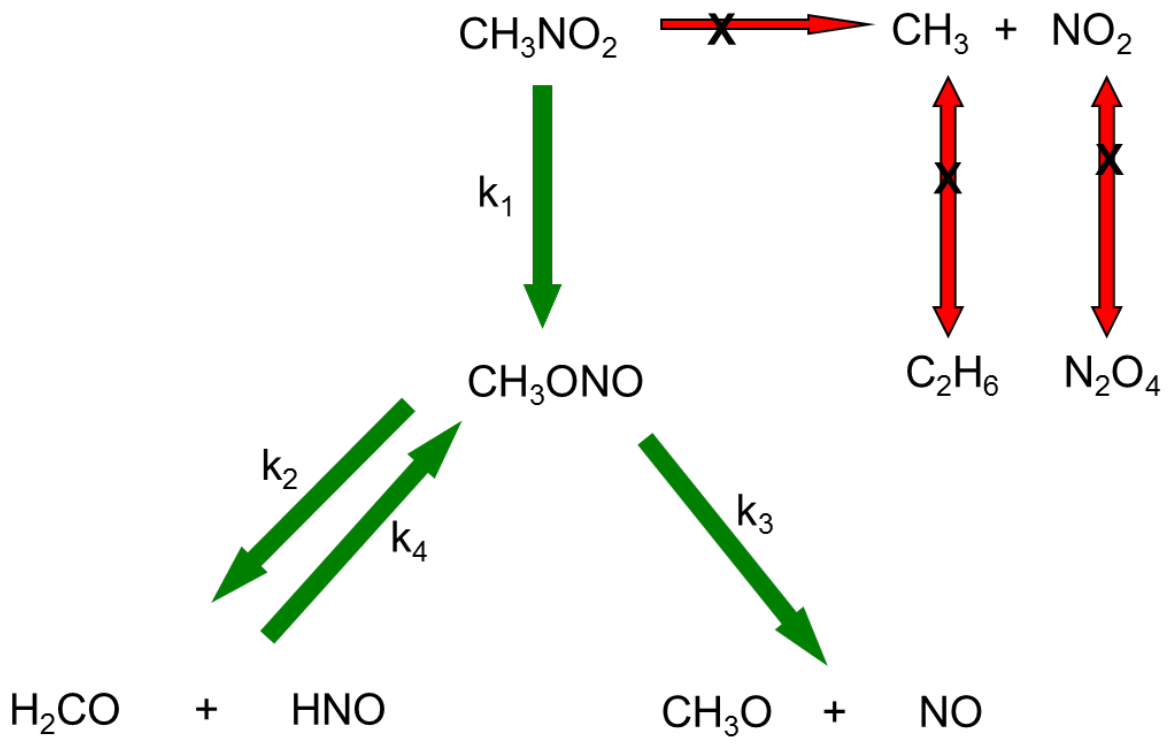

Figure 4. Kinetic scheme to fit the temporal evolution of the newly formed molecules shown in Figures 3A and 3B.

4.1. Mass Spectroscopy

Reflectron time-of-flight mass spectroscopy coupled to single photon ionization ('soft photoionization') (ReTOF-PI) upon sublimation of the irradiated ices presents a unique advantage compared to traditional mass spectroscopy coupled with electron impact ionization at, for instance, 100 eV ('hard ionization). In principle, *any* molecule can be ionized by electron impact. Traditionally, the ionization of neutral molecules is conducted at electron energies between typically 80 eV and 100 eV (*hard* electron impact ionization), i.e. the range where the ionization cross section of organic molecules is at the maximum. However, at these electron energies, molecules undergo extensive dissociative ionization yielding significant fragment ions. In the extreme case, this can even result in a situation in which the parent ion depicts only a few percent of the total ion count or is even unstable (no signal count for the parent ion).

On the other hand, *soft* ionization exploiting tunable, fragment-free vacuum ultraviolet (VUV) single photon ionization can eliminate the problem of dissociative ionization and the interfering species. In most of the cases VUV photoionization only results in the formation of parent ion of the product molecule without forming fragment ions thus essentially eliminating dissociative ionization. Most importantly, by selectively tuning the ionization energy above the ionization energy of one molecule, but below the ionization energy of a second molecule, isomers can be ionized selectively.

This is of particular relevance to the present system. After the electron exposure of the icy films, the irradiated (D3)-nitromethane samples are warmed up with 0.5 K min^{-1} to 300 K. As pictured in Figure 1B, the photoionization laser (10.49 eV) interrogates the subliming molecules almost perpendicularly above the silver target. The resulting ion currents as a function of temperature and mass-to-charge are compiled for all systems in Figure 5. Here, the subliming nitromethane (CH_3NO_2) cannot be photoionized since its ionization energy (11.08 eV) is above the energy of the photoionization laser. On the other hand, the methylnitrite (CH_3ONO), which presents the isomerization product of nitromethane, holds an ionization energy of only 10.44 eV and can be photoionized. Therefore, ion signal at mass-to-charge of 61 can *only* originate from CH_3ONO^+, but *not* from $CH_3NO_2^+$ (Table 3).

The individual TOF spectra are compiled in Figure 6 with masses listed and cross linked to their deuterated counterparts in Table 3. Nitrogen monoxide could be identified via its parent ion in all systems at m/z = 30. Nitrosyl hydride (HNO) and its deuterated counterpart could be probed at m/z = 31 (HNO^+) and 32 (DNO^+), respectively. The methylnitrite isomer (CH_3ONO) and its ^{13}C substituted counterpart ($^{13}CH_3ONO$) were detected at m/z = 61 and 62, respectively. The shift by three amu in the D3-nitromethane sample rises to ion counts at m/z = 64 and 65 for CH_3ONO and $^{13}CH_3ONO$, respectively. Note that the ionization energy of formaldehyde (H_2CO; 10.88 eV) is above the energy of the ionization laser.

However, the appearance of additional ion peaks with up to 75 amu, which cannot be linked to the infrared spectroscopically derived reaction pathways as compiled in Figure 4, clearly indicates a more complex chemistry in the condensed phase than previously thought. The data analysis of these TOFs is still ongoing, so only a preliminary analysis is given here. First, the TOFs at m/z = 33 (H_2NOH^+) and 36 (D_2NOD^+) propose the existence of free (suprathermal) hydrogen atoms, which can hydrogen atoms which can hydrogenate the nitrosyl hydride molecule (HNO). Second, the detection of signal at m/z = 45 and the corresponding shift to m/z = 48 indicated a system with three hydrogen atoms, i.e. H_2CNOH and/or CH_3NO. The latter might be formed as a

Table 3. Assignment of the ion peaks observed in the sublimation profiles of the irradiated D3- and CH_3NO_2 ices. ? Hitherto unassigned..

Ion signal (m/z)	Assignment	Ionization Energy (eV)	Ion signal (m/z)	Assignment
30	NO	9.26	30	NO
31	HNO	10.10	32	DNO
33	H_2NOH	10.00	36	D_2NOD
44	?			
45	H_2CNOH/ CH_3NO	10.16/9.30	48	D_2CNOD/ CD_3NO
46	?		?	
47	CH_3NHOH	9.55	52	CD_3NDOD
58	?		?	
59	?		?	
60	?		?	
61	CH_3ONO	10.44	64	CD_3ONO
62	$^{13}CH_3ONO$	10.44	65	$^{13}CD_3ONO$
75	?		?	

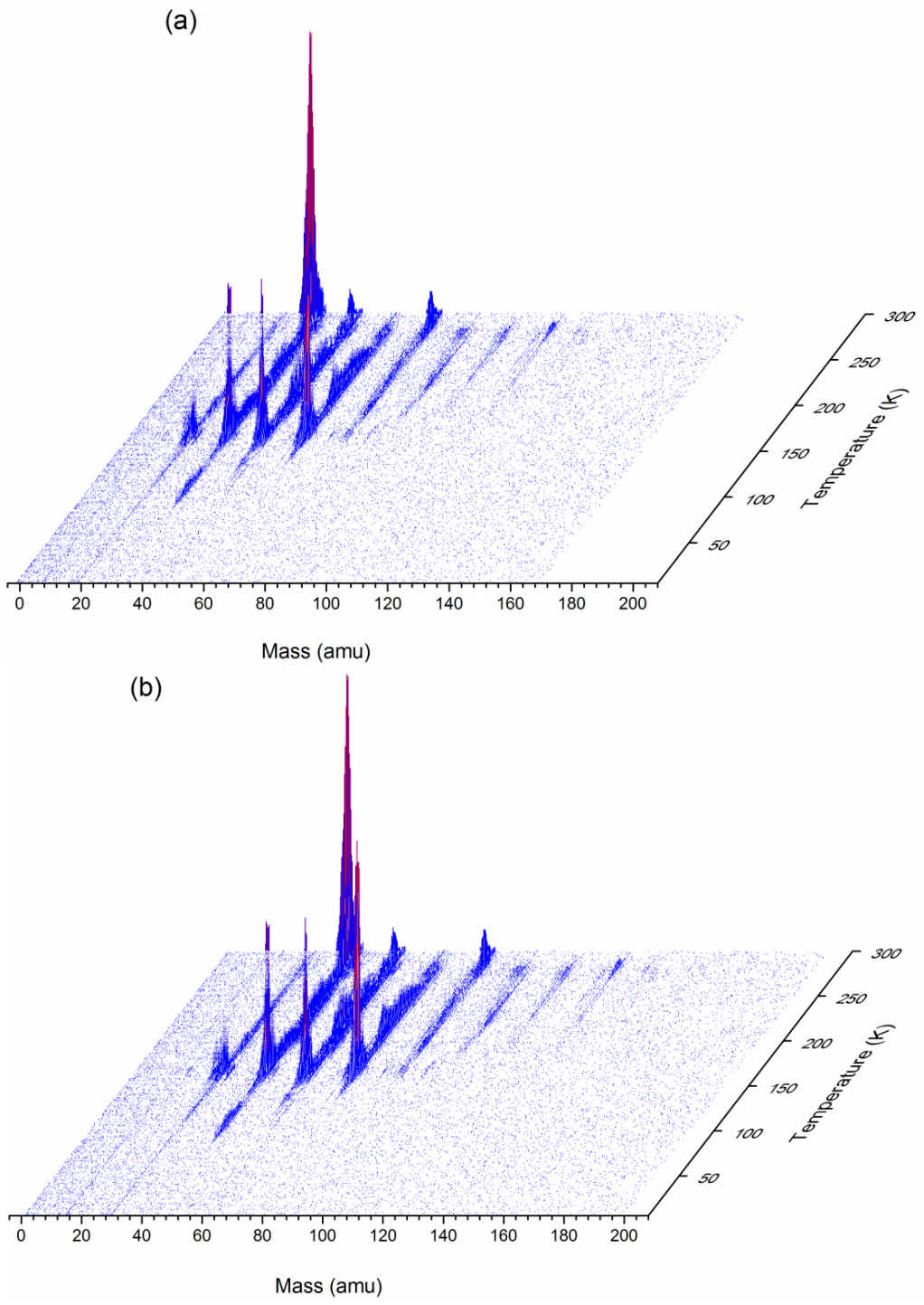

Figure 5A. ReTOF-PI spectra as a function of temperature of the newly formed products subliming into the gas phase from the irradiated nitromethane (CH_3NO_2) ices with irradiations conducted at 50 nA (a) and 100 nA (b).

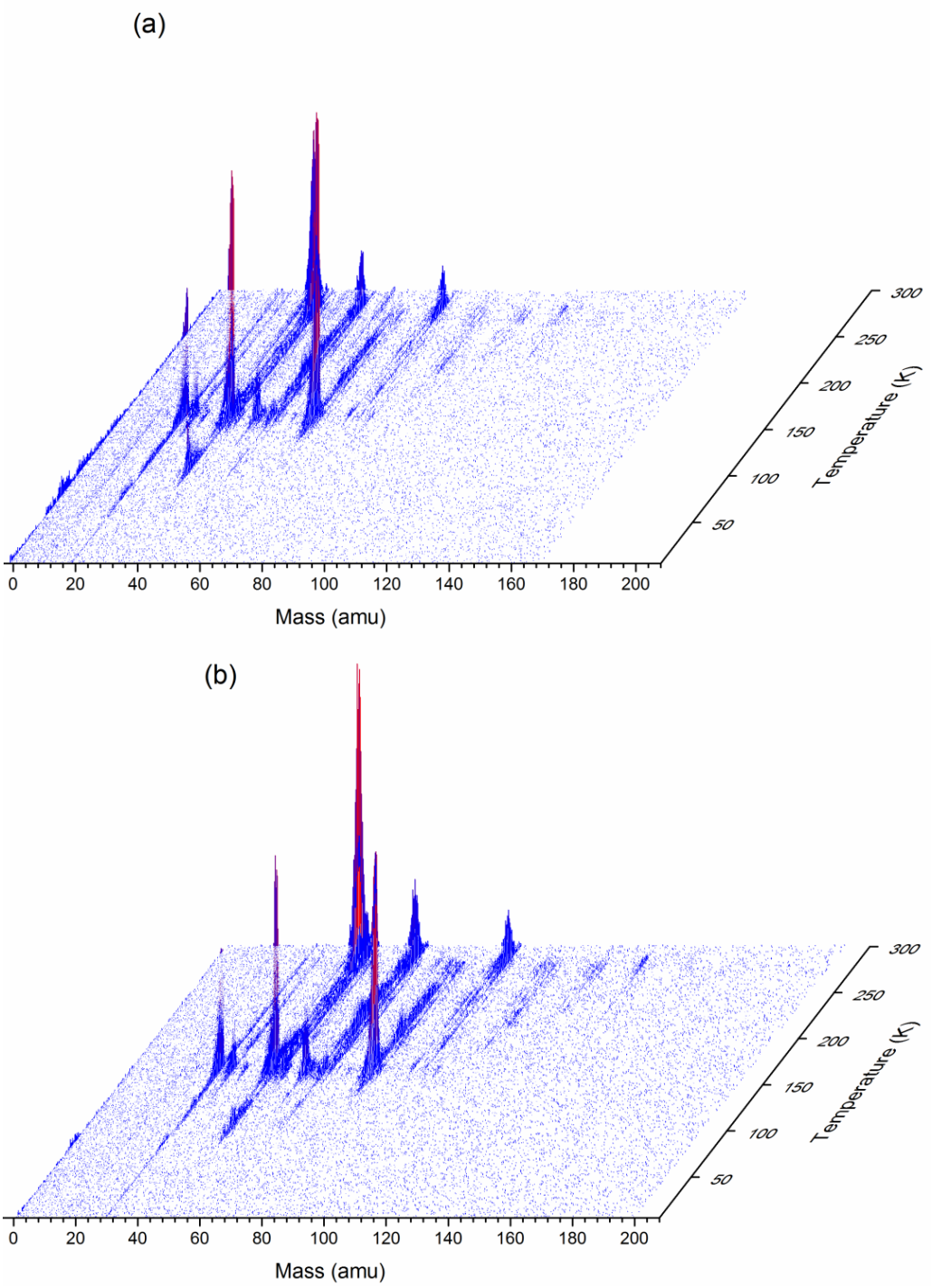

Figure 5B. ReTOF mass spectra as a function of temperature of the newly formed products subliming into the gas phase from the irradiated D3-nitromethane (CD_3NO_2) ices with irradiations conducted at 50 nA (a) and 100 nA (b).

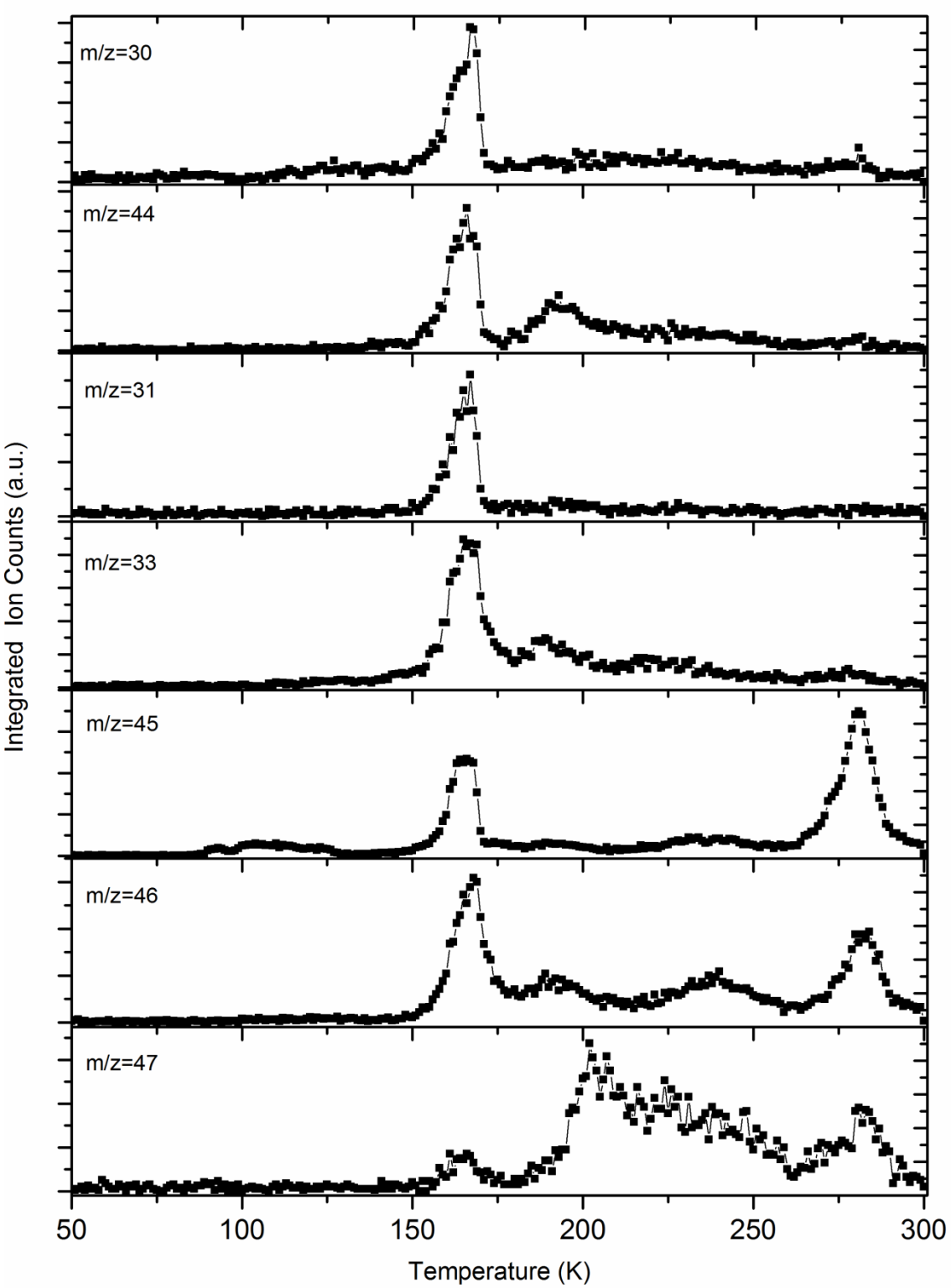

Figure 6A. ReTOF spectra of the newly formed products as a function of temperature subliming into the gas phase from the irradiated nitromethane (CH_3NO_2) ices.

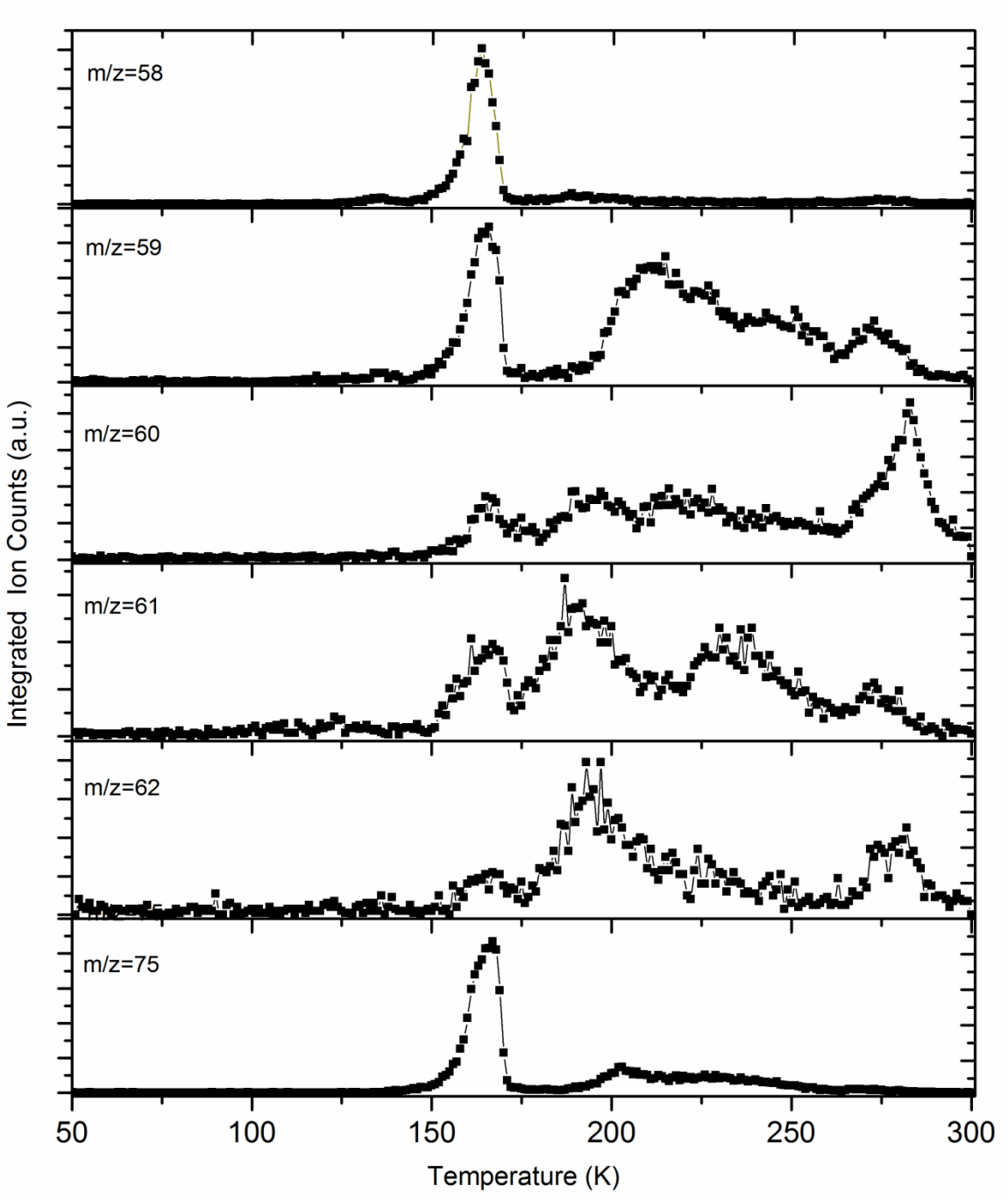

Figure 6A. (continued)

4. Summary

We presented a preliminary data analysis of the electron-induced decomposition of nitromethane (CH_3NO_2) in the condensed phase at 5 K. The following findings shall be highlighted.

1. Infrared spectroscopically, we have identified four newly formed molecules in irradiated (D3)-nitromethane ice films: CH_3ONO, H_2CO, NO, and HNO.

2. We also elucidated the underlying formation pathways by tracing the temporal profiles of the bands during the irradiation and numerically fitting these temporal profiles.

3. The data analysis suggest (pseudo) first order kinetics of the formation of methyl nitrite (CH_3ONO) via isomerization of nitromethane (CH_3NO_2) (k_1) in the condensed phase. In the gas phase, this pathway has been proposed to involve a roaming-mediated isomerization via an initial carbon-nitrogen bond rupture. However, in the condensed phase, both the methyl radical and the nitrogen dioxide formed via the carbon-nitrogen bond rupture are trapped within the matrix cage and can recombine back either to nitromethane (CH_3NO_2) or methyl nitrite (CH_3ONO). ***In the condensed phase, roaming reaction dynamics are not required to explain the experimental data***. The isomerization of D3-nitromethane is surprisingly ***faster*** than of nitromethane with $k_1(CD_3NO_2)/k_1(CH_3NO_2) = 2.0 \pm 0.8$. This proposed non-equilibrium reaction dynamics in the condensed phase. This 'cage effect' is reflected in reaction mechanisms, which do not exist in gas phase reactions under single collision conditions, where the nascent products 'fly apart' or undergo prior reactions via 'roaming'.

4. No evidence of a unimolecular decomposition of nitromethane (CH_3NO_2) leading to free methyl radical (CH_3) and nitrogen dioxide (NO_2) was observed. Therefore, the nitromethane – methyl nitrite isomerization represents the exclusive, initial reaction step in this system. This is in strong discrepancy to the unimolecular decomposition of nitromethane in the gas phase, where the carbon-nitrogen bond is split, and the methyl radical (CH_3) and nitrogen dioxide (NO_2) products fly apart undisturbed. Infrared multi photon (IRMPD) and ultraviolet photodissociation (UVPD) of nitromethane (CH_3NO_2) have been exploited for years. In a pioneering molecular beams experiment by Lee et al., infrared multi photon dissociation studies utilizing the 10.6 μm output of a carbon dioxide laser suggested the existence of two processes via carbon-nitrogen and oxygen-nitrogen bond cleavage processes, i.e. the channels $CH_3 + NO_2$ and $CH_3O + NO$ with the latter being dominant involving the methyl nitrite isomer (CH_3ONO). Follow up experiments at 193 nm indicated that the cleavage of the carbon-nitrogen bond and production of the methyl radical (CH_3) plus nitrogen dioxide (NO_2) was the primary process. In the condensed phase, however, the initial fragments are hindered by the matrix cage and hence react back either to nitromethane (CH_3NO_2) or isomerize to methyl nitrite (CH_3ONO).

5. Methyl nitrite (CH_3ONO) was found to decompose via two competing pathways into formaldehyde (H_2CO) plus nitrosyl hydride (HNO) and the methoxy radical (CH_3O) plus nitrogen monoxide (NO) with rate constants k_2 and k_3, respectively. The fits propose that both in the nitromethane and D3-nitromethane systems, the molecular product channel (k_2) dominates with branching ratios of $(3.0\pm0.8) : 1$ and $(5.0\pm1.5) : 1$, respectively. ***The dominance of the molecular product channel is quite distinct from the gas phase experiments depicting a prevailing radical channel (Bowen et al. JPCA 117, 11665-11672).***

5. Future Plans

We are planning to expand the research on the following levels:

L1: To finalize the data analysis of the electron induced decomposition of (D3) nitromethane (CH_3NO_2) in the condensed phase and to disseminate the results.

L2: To start the data analysis of Lyman α (10.49 eV) photolyzed (D3) nitromethane (CH_3NO_2) ice films.

L3: To engage a collaboration with Joel Bowman (Emory) on the Lyman α experiments and to compare our experimental branching ratios with those obtained from calculations on photolyzed nitromethane clusters.

L4: To disseminate the findings via two peer-reviewed publications.